This is a preprint, the final version is subject to change, of the American Mineralogist (MSA)
Cite as Authors (Year) Title. American Mineralogist, in press.
(DOI will not work until issue is live.) DOI: http://dx.doi.org/10.2138/am.2014.4658

Revision 1

Transformation of graphite to diamond via a topotactic mechanism

Laurence A.J. Garvie[1], Péter Németh[2,3] and Peter R. Buseck[3,4]

[1]*Center for Meteorite Studies, Arizona State University, Tempe, Arizona 85287-6004, USA.*

[2]*Institute of Materials and Environmental Chemistry, Research Center for Natural Sciences, Hungarian Academy of Sciences, H-1025 Budapest, Pusztaszeri út 59-67, Hungary.*

[3]*School of Earth and Space Exploration, Arizona State University, Tempe, Arizona 85287-6004, USA.*

[4]*Department of Chemistry and Biochemistry, Arizona State University, Tempe, AZ 85287-1604, USA.*

ABSTRACT

Several mechanisms and intermediate steps have been proposed to explain the transformation of graphite to diamond. However, the mechanism continues to be debated, in part because graphite that is incompletely transformed to diamond has not been reported; although such material could be used to better understand the diamond-forming process. Here we report the discovery of nano-sized grains of interstratified graphite and diamond from Gujba, an extraterrestrially shocked meteorite. We use high-resolution transmission electron microscopy (HRTEM) data from these grains to show that diamond formed via a reconstructive, topotactic rather than martensitic mechanism. Electron diffraction and HRTEM images show the following three-dimensional crystallographic relationships between the interstratified graphite and diamond: $[001]_g$ || $[111]_d$, $[100]_g$||$[2\text{-}1\text{-}1]_d$ and $[1\text{-}20]_g$||$[0\text{-}11]_d$. These relationships yield the transition matrix linking the graphite and diamond unit cells, which become

coincident for graphite compressed to 7 GPa. The specific product, whether single-crystal or twinned diamond is dictated by the initial graphite polytype and transformation route. The derivation of a three-dimensional transition matrix is consistent with a topotactic relationship between graphite and the newly formed diamond.

Key Words: Crystal Structure, Crystal Growth, Electron Microscopy, Meteorite

INTRODUCTION

Shock waves can convert carbonaceous materials to diamond. Products of this process occur as the result of explosive compression of powders (DeCarli and Jamieson 1961; Donnet et al. 2000; Donnet et al. 1997; Erskine and Nellis 1991; Yamada et al. 2000), extraterrestrial impacts (Le Guillou et al. 2010; Sharp and DeCarli 2006), and impacts of meteors on Earth (El Goresy et al. 2001; Langenhorst et al. 1999; Pratesi et al. 2003; Yelisseyev et al. 2013). Of particular interest are the recent reports of terrestrial impact-produced nanodiamonds, specifically those associated with the hypothesized Younger Dryas (YD) boundary impact event (Israde-Alcantara et al. 2012; Kennett et al. 2009a; Kennett et al. 2009b; Kurbatov et al. 2010). These reports describe nanodiamonds, diamond, lonsdaleite, and n-diamond, in sediments of the Ållerød-Younger Dryas boundary, with the lonsdaleite being presented as evidence of shock synthesis (Kennett et al. 2009a; Kennett et al. 2009b), although the evidence for lonsdaleite in these deposits is open to debate (Daulton et al. 2010). In order to use the presence and characteristics of the shock-formed diamonds as indicators of specific formation processes, it is necessary to understand the mechanisms and conditions under which graphite transforms to diamond.

Graphite has been proposed to form diamond through either a martensitic or reconstructive process, whereas non-graphitic carbon such as carbon black and glassy carbon transforms to diamond by a reconstructive mechanism (Irifune

and Sumiya 2004; Le Guillou et al. 2007; Sumiya et al. 2006). Static and shock wave experiments show that the uncatalyzed, direct transformation of graphite to diamond requires pressures >15 GPa and transient T of >3000 K (reviewed in (DeCarli 1995; DeCarli et al. 2002)). Shock-wave experiments suggest that graphite oriented with its basal planes normal to the direction of shock-wave propagation transforms to diamond through a two-step martensitic mechanism (Erskine and Nellis 1991; Erskine and Nellis 1992): graphite to lonsdaleite (also called hexagonal diamond), followed by a transformation from lonsdaleite to diamond at < 2000 K, substantially below the melting temperature of graphite. Independent of the mechanism by which it occurs, the transformation results in a 61% collapse along the [001] of graphite, whereas the lateral dimensions decrease by only 2.8%. Strong covalent bonds form in diamond, and there is a dramatic density increase from 2.28 to 3.52 g/cm^3. The bonding changes from planar, 3-coordinated, sp^2-bonded C in sheets held together by Van der Waals forces for graphite to 4-coordinated, sp^3-bonded C in diamond. Also, the planar C-C bond length of graphite increases by 0.015 nm on transforming to diamond.

A range of intermediates structures have been hypothesized to form during shock or static compression of graphite to diamond (Khaliullin et al. 2011; Le Guillou et al. 2007; Yang and Wang 2001) starting with the two major graphite polytypes: 2H (hexagonal, AB stacking) and 3R (rhombohedral, ABC stacking). 3R graphite is thought to form diamond via buckling and compression of graphene sheets, without the formation of intermediate structures, whereas diamond formation from the 2H polytype proceeds through intermediate structures that transform first to lonsdaleite and then to diamond (Khaliullin et al. 2011; Le Guillou et al. 2007; Scandolo et al. 1995).

As part of our ongoing study of the fine-grained materials in carbonaceous chondrite meteorites, we used transmission electron microscopy (TEM), selected-area electron diffraction (SAED), and electron energy-loss spectroscopy (EELS) to investigate the acid-insoluble material from Gujba, in

which we discovered grains of graphite and diamond. Gujba is a coarse-grained carbonaceous chondrite meteorite that consists predominantly of silicate clasts, large metal globules, and dark interstitial matrix (Figs. 1 and 2) (Rubin et al. 2003) that shows a range of shock features. The whole rock shows evidence of shock stage S2 (Rubin et al. 2003). Features indicating high shock pressures are evident in the matrix, which consists of fine-grained metal and silicate that resembles the shock veins in ordinary chondrites. Several high-pressure, presumably shock-produced, phases occur in Gujba including majorite garnet, wadsleyite, and coesite (Weisberg and Kimura 2004; Weisberg et al. 2006), and stishovite (this study). The wadsleyite and majorite indicate maximum local pressures and temperatures of 19 GPa and 2000 °C. There are no prior reports of diamonds in Gujba, but they were described from Bencubbin, where some are thought to have formed via solid-state transformation of carbon from an intense shock event, with peak pressure exceeding 15 GPa (Mostefaoui et al. 2002).

Here we show images of graphite in the process of transforming to diamond. From these images we derive a three-dimensional transition matrix linking the unit cells of graphite and diamond, and conclude that the transformation proceeds through a reconstructive, topotactic mechanism.

EXPERIMENTAL METHOD

Several millimeter-sized pieces of black areas interstitial to the large metal and silicate globules were separated from a piece of the Gujba meteorite (Fig. 2). These pieces were washed in 6N HCl for two days, then three days in HF/HCl, followed by three washes in dilute HCl, and final washings in distilled water. The dissolution was undertaken at room temperature. A small droplet (ca. 2 μL) of the residue in suspension with water was dried on a Cu TEM grid coated with lacy-C. TEM data were acquired from electron-transparent areas of the residue protruding into the holes of the TEM grid. EELS and SAED data were acquired with a Tecnai F20 TEM (200 *kV*; Schottky field-emission gun, side-entry, double-

tilt stage; point resolution = 0.24 nm). HRTEM images were acquired with a JEOL JEM 4000EX TEM (400 kV; LaB_6 filament, top-entry, double-tilt stage; C_s = 1 mm; point resolution = 0.17 nm). Fourier-transform diffractograms obtained from the HRTEM images were calculated using Gatan Digital Micrograph 2.5.7 software. Structure models of transitional graphite diamond and HRTEM images were simulated with Cerius2 4.0 software (Molecular Simulation Institute, Inc) at the microscope experimental conditions (defocus spread = 7 nm, beam divergence = 0.4 mrad, defocus = - 40 nm, and sample thickness = 5 nm). Structure data for diamond (F 3dm) and graphite (2H $P6_3/mmc$ and 3R R-3m) are taken from (Lipson and Stokes 1942; Wyckoff 1963). We used the CrystalCracker software to calculate the unit cell parameters of diamond by applying the transition matrix developed in this paper (http://multianvil.asu.edu/Crystal_Cracker/CrystalCracker.html).

RESULTS AND DISCUSSION

TEM images of the acid residue show abundant carbonaceous aggregates and lath-shaped stishovite (Fig. 3). A combination of high-resolution TEM (HRTEM), SAED, and EELS measurements from multiple carbonaceous aggregates reveal particle types that range from amorphous to poorly graphitized carbon (PGC), to well-ordered graphite, rounded to euhedral diamonds, and clumps of nanodiamonds. Hollow carbonaceous nanoglobules also occur (Fig. 3), similar to those in primitive meteorites (Garvie and Buseck 2004; Nakamura-Messenger et al. 2006), and structurally similar PGC occurs in many carbonaceous chondrites (Garvie and Buseck 2006; Harris and Vis 2003).

Notable aspects of some HRTEM images are platy grains (Fig. 4), typically 15 x 8 nm, rarely up to 50-nm long that show various proportions of 0.34-nm fringes and parallel 0.206-nm fringes (Figs 4, 5 and 6). Approximately 100 carbonaceous aggregates containing such elongated particles were imaged, with some aggregates containing up to 35 grains. Their SAED patterns contain rings

corresponding to graphite and diamond (Fig. 4b), and the C K edge EELS spectra has maxima for these minerals (Fig. 4c) (Garvie 2006). The 0.34-nm fringes are consistent with 2H (002) and 3R (003) graphite, and the 0.206-nm fringes, which lie parallel to the graphite 00*l* fringes (Figs. 5 and 6), are of diamond (111).

The proportions of diamond vary in different grains (Fig. 5). Some consist of interstratified blocks of diamond and books of graphite (Fig. 5a), whereas others show diamond on one surface (Fig. 5). Some grains show extensive layers in which graphite appears to grade into diamond (yellow arrowed regions in Figs. 5 and 6). Some crystallites show 0.34-nm spacings that transition to material with 0.206-nm spacings. [001] line dislocations and (001) stacking faults are abundant in the graphite, and much of the diamond is twinned (Figs. 5 and 6). The HRTEM images reveal two graphite polytypes: 3R with 0.34-nm (003) and 0.21-nm (-101) spacings, and 2H with 0.34-nm (002) and 0.21-nm (100) spacings. Diamond shows 0.206-nm (111 and 1-1-1) spacings.

In order to understand the structure at the junction between diamond and graphite, the intermediate graphite diamond region in Figure 6 (indicated by the yellow arrow) was modeled using the structures of diamond and 3R graphite, and simulated HRTEM images were generated (Fig. 7). At the imaging conditions used, the black dots correspond to C doublets. The high point-to-point resolution provides images that permit us to determine the orientations of these doublets and hence the atomic structure of the graphite-diamond interface.

We use two model structures for the interstratified graphite diamond region in Figure 6, one with a graphite layer and the other with a diamond layer at the interface. Both are required since the intensity differences at this region of the simulated HRTEM images for the two structures are not sufficient to determine whether the interface is graphite (Fig. 7d) or diamond (Fig. 7e).

The models have in common an upper and lower part of diamond (111) planes separated by a 0.34-nm spacing, and the C doublets are in a twin relation (Fig. 7d, e). The model also shows a defect between the twinned regions of the

diamond (black arrow) that is offset by 0.17 nm. The twinning is also visible in the HRTEM image (black boxed region in Fig. 6a). The connection between the upper and lower diamond layers (arrows in Fig. 7d, e) is neither pure diamond nor graphite, but retains appropriate C-C bond distances and angles between that of graphite and diamond.

The HRTEM images and calculated diffractograms from the Gujba meteorite reveal the orthogonal crystallographic relationships between the graphite and diamond: $[001]_g||[111]_d$, $[100]_g||[2\text{-}1\text{-}1]_d$ and $[1\text{-}20]_g||[0\text{-}11]_d$. The orientation relationships in Figure 6 are typical of the grains showing interstratified blocks of diamond and books of graphite. These orientations uniquely define the three-dimensional relationship between the graphite and the newly formed diamond. The one dimensional $[001]_g || [111]_d$ relationship is well-known, and more recently (Nakamuta and Toh 2013) suggested further orientation relationships between graphite and newly formed diamond. However, determination of the three-dimensional directional relationship was only possible because of the preservation of the intergrown diamond and graphite in the Gujba meteorite.

The measured orthogonal orientational relationships $[001]_g || [111]_d$, $[100]_g||[2\text{-}1\text{-}1]_d$, and $[1\text{-}20]_g||[0\text{-}11]_d$, and reciprocal lattice node overlaps allow development of the respective transition matrices (Appendix 1) between 2H and 3R graphite and the newly formed diamond. The unit cells of 2H and 3R graphite transform to diamond through

$$\frac{1}{3}\begin{pmatrix} 4 & 2 & 1 \\ -2 & 2 & 1 \\ -2 & -4 & 1 \end{pmatrix} \text{ and } \frac{2}{9}\begin{pmatrix} 6 & 3 & 1 \\ -3 & 3 & 1 \\ -3 & -4 & 1 \end{pmatrix}, \text{ respectively.}$$

Application of the matrices to the room-pressure 2H and 3R graphite unit cells give a slightly distorted pseudo-cubic diamond unit cell, with a= 0.36 nm and

alpha= 85.8°. However, with increasing pressure graphite compresses dramatically along *c*, with only minor changes along *a* (Yagi et al. 1992). Application of the matrices to the unit-cell data for graphite at approximately 7 GPa, where the c/c_0 ratio decreases to 0.91 (Yagi et al. 1992), yields cell data consistent with diamond. Although 7 GPa is within the stability field for diamond for T~<3,000K, the conversion of graphite to diamond requires pressures above ~10 GPa (Bundy et al. 1996). Below 10 GPa the conversion is kinetically inhibited.

Our data are consistent with graphite transforming to diamond, as opposed to diamond to graphite. HRTEM images of diamond transforming to graphite do not show a crystallographic relationships between the newly formed graphite and parent diamond structure (Mykhaylyk et al. 2005; Zou et al. 2010). Further, the interstratified graphite-diamond grains are platy, suggestive of a platy graphite precursor.

There are many possible graphite polytypes, however, 3R and 2H are the most abundant. Moreover, longer-period graphite polytypes can be envisioned as consisting of 2H and 3R, showing that all graphite polytypes can transform via the paths outlined in Figure 8. Starting with the 3R and 2H graphite polytype, we propose several paths to diamond. 3R graphite can transform either by maintaining its original stacking sequence (Fig. 8 path a) or through intermediate graphite stackings I1 and I2 (Fig. 8 path b). On the other hand, 2H can transform through either 3R graphite (Fig. 8 path c) or intermediate stackings (Fig. 8 path d). The intermediate structures with AB'AB' (I1, also called orthorhombic graphite (Khaliullin et al. 2011; Scandolo et al. 1995)) and AAAA (I2, termed 1H graphite (Le Guillou et al. 2007)) stacking sequences have been hypothesized as intermediates in the graphite-diamond transition. These intermediates are the most fundamental stackings that can transform to diamond (Fig. 8 path f). However, a range of different stacking sequences can be envisioned (e.g., AB'B'A, AB'CCB'A etc…) that will only produce different diamond stacking

(e.g., 4H or 6H). These stackings will, in turn, form diamond with planar defects, resulting in twinning. Therefore, the abundance of twinned diamond in our sample is likely related to the stacking disorder of the original graphite, intermediate paths, or both.

The crystallographic relationship between graphite and diamond, and the existence of a corresponding transition matrix, is consistent with both topotactic and martensitic transitions. In a topotactic transition the "... crystal lattice of the product phase shows one or more crystallographically equivalent, orientational relationships to the crystal lattice of the parent phase." (IUPAC 1997), which according to Sharp and DeCarli (2006) is a type of reconstructive phase transition. Whereas, a martensitic transition is a "... diffusionless transition ... generated by coordinated atomic ... displacements over distances smaller than interatomic distances in the parent phase." (IUPAC 1997). Although the graphite to diamond transition is commonly described as martensitic, the transition as a whole is not. In particular, the atomic displacements are larger than the interatomic distances in the parent phase, e.g., the 0.34 nm of graphite becomes the 0.156 nm of diamond. As a whole, the structural changes and resultant chemical and physical differences, such as density increase between graphite and diamond, are consistent with a reconstructive, topotactic rather than a martensitic transition.

Our study outlines transformation routes for the formation of diamond from graphite that are consistent with grains consisting of interstratified blocks of diamond and books of graphite. The discovery of the three-dimensional transition matrix supports a reconstructive, topotactic transformation between graphite and diamond as a result of shock-induced phase change. The results presented here are also applicable to static high-pressure experiments as there is no evidence to suggest that the physics, and hence outcomes, of static and shock experiments differ, e.g., see discussions in Sharp and DeCarli (Sharp and DeCarli 2006). The HRTEM images also show grains where diamond formation appears

to have stopped at dislocations, which suggest that defects can impede diamond formation and result in regions with intimately intergrown graphite and diamond. Defects may also be important for initiation of the phase transformation (Khaliullin et al. 2011; Le Guillou et al. 2007) as they are postulated to be the sites for initiation of the diamond formation through dangling bonds. The findings provide new mechanistic insights into the interactions that control the transformation of graphite into diamond.

ACKNOWLEDGMENTS

We are grateful to the staff and for use of the facilities in the John M. Cowley Center for High Resolution Electron Microscopy at Arizona State University. L.A.J.G was supported by NASA Origins of Solar Systems grant NNX11AK58G and P.N. acknowledges support from Hungarian Scientific Research Fund and Hungarian Economic Development Centre grant HUMAN_MB08-1-2011-0012. The work at ASU was also supported by Cosmochemistry grant NNX10AG48G. The authors are grateful to the associate editor Ian Swainson, and the three reviewers (A. El Goresey and two anonymous), for their insightful comments and suggestions.

FIGURE 1. A polished and nitol-etched piece of the Gujba meteorite showing the bright metal globules and interstitial silicate fragments and dark matrix. The piece measures 3 cm across. The largest metal globule is just under 5 mm in diameter. (sample ASU#1660)

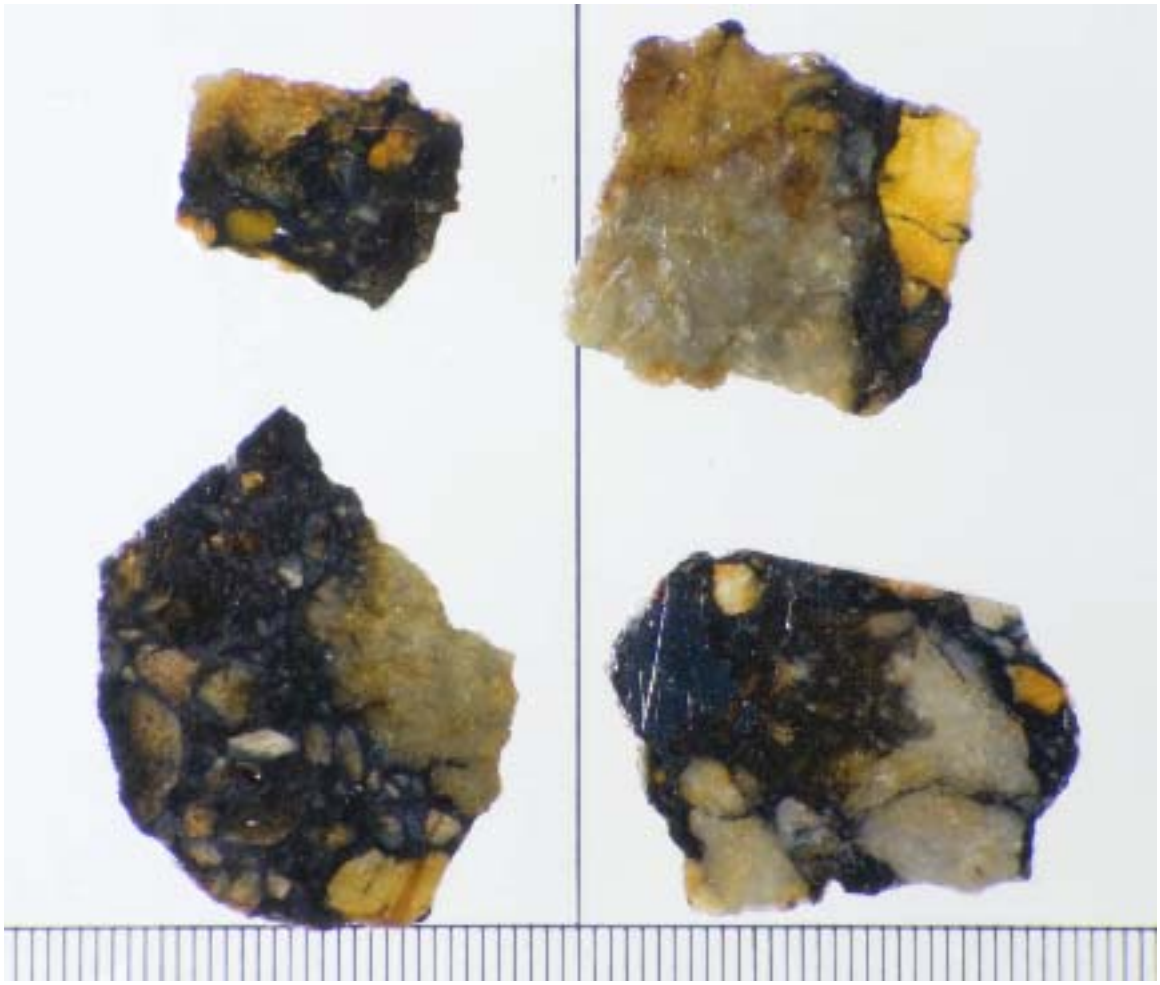

FIGURE 2. Photograph of representative pieces of material interstitial to the metal globules showing the light-colored silicate fragments, metal, and dark-veined material. The dark areas are dominated by metal, sulfides, and carbonaceous material. The scale bar markers at the bottom of the image = 0.2 mm.

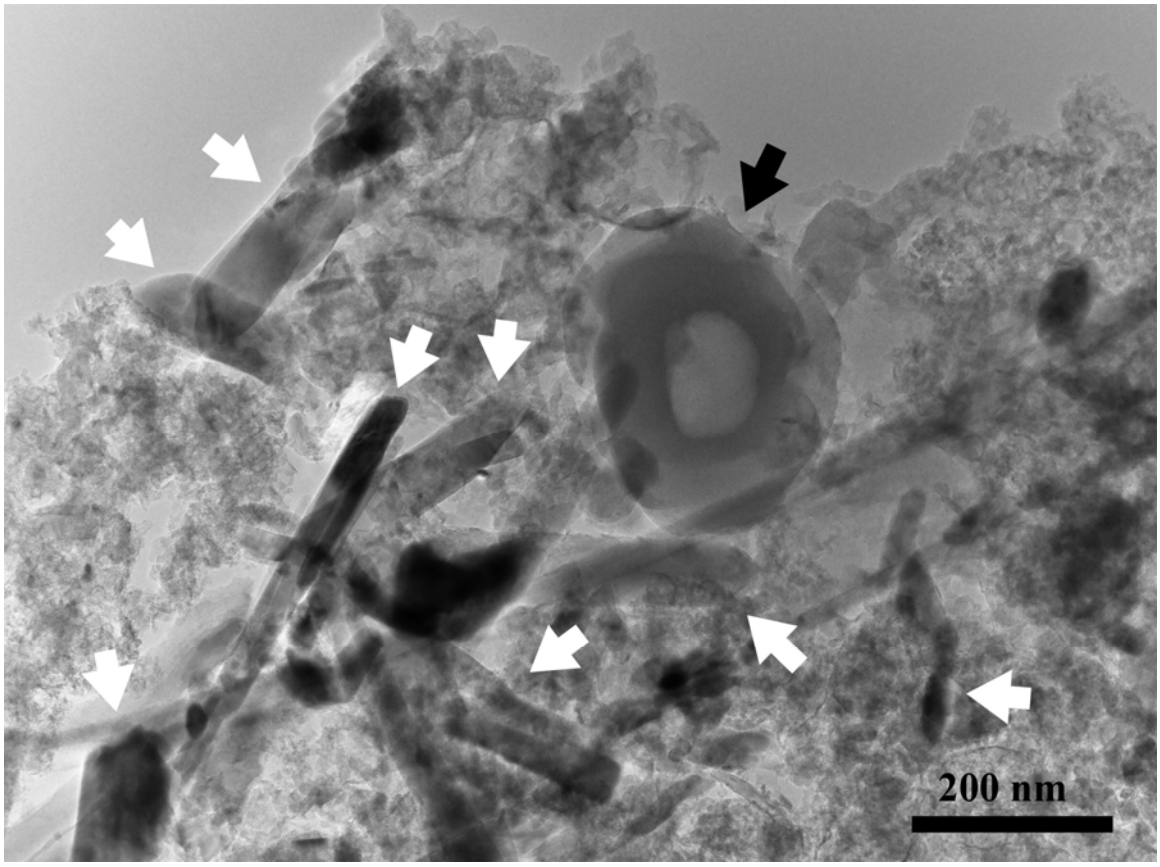

FIGURE 3. Low-resolution TEM image of the acid residue from Gujba showing a hollow carbonaceous nanoglobule (black arrow) and stishovite laths (white arrows). The formless, tissue-like material forming the bulk of the residue is a mixture of poorly graphitized carbon, graphite-diamond, and diamond.

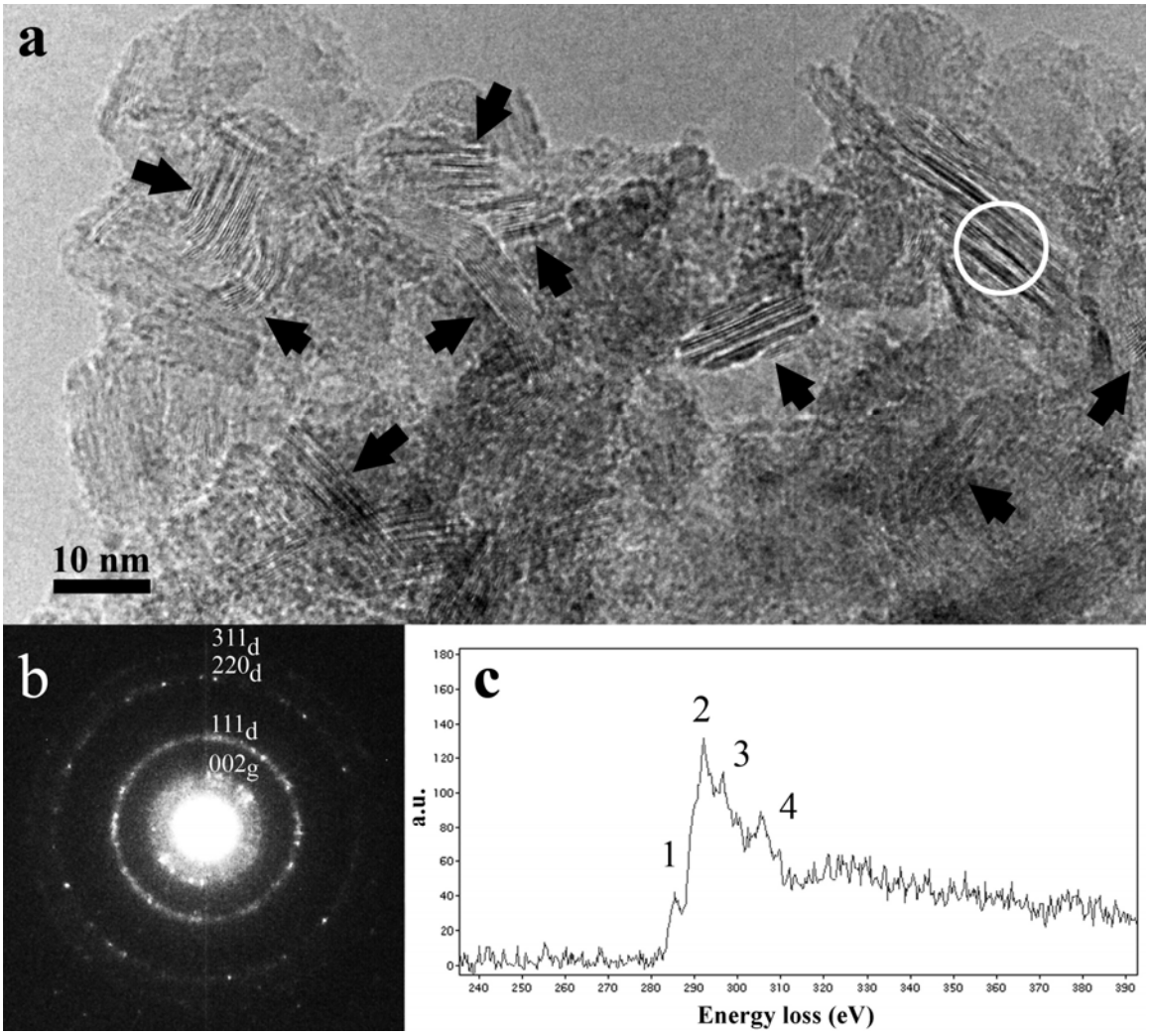

FIGURE 4. Low-resolution TEM image of a cluster of graphite-diamond particles **(a),** with corresponding SAED pattern **(b),** and EELS spectrum **(c)**. The arrows on the TEM image point to individual graphite-diamond crystallites that are oriented to show 0.35- (graphite) and 0.21- nm (diamond) fringes. The SAED pattern was acquired from the whole region in **(a)** and shows rings for graphite (subscript g) and diamond (subscript d). Only the most intense ring of 2H graphite is indexed. The EELS spectrum was acquired from the area indicated by the white circle in **(a)**. The EELS spectrum **(c)** shows a C K edge with a π* peak for graphite (peak 1), a composite graphite and diamond maximum (peak 2), and maxima for diamond (peaks 3 and 4).

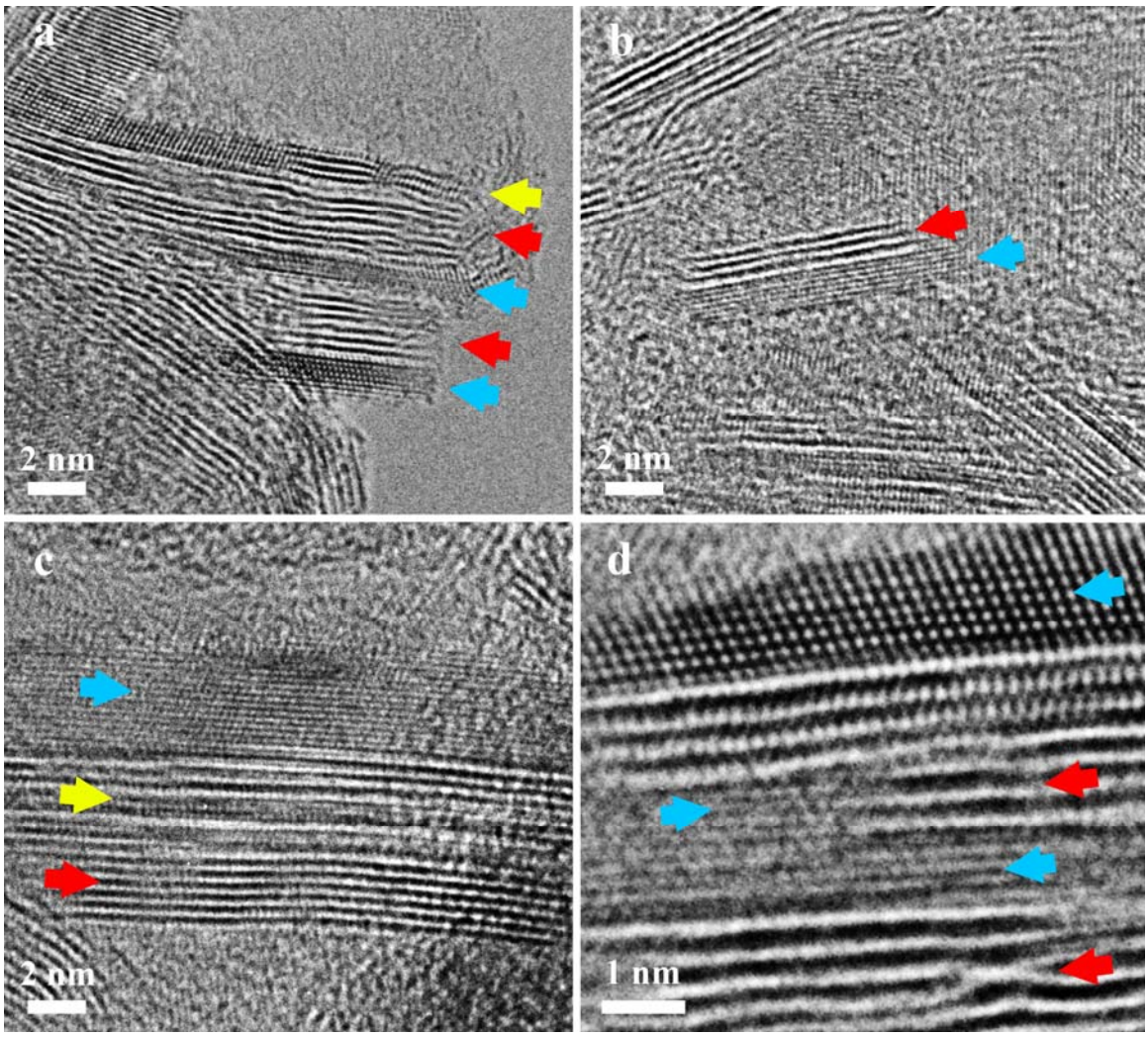

FIGURE 5. Representative HRTEM images of individual graphite-diamond crystallites. **(a)** Interstratified graphite (red arrows) and diamond (blue arrows). The yellow arrow indicates where graphite (00*l*) and diamond (111) fringes meet. **(b)** Cluster of crystallites. **(c)** Crystallite showing clearly resolved graphite and diamond fringes separated by layers with poorly resolved fringes (yellow arrow). **(d)** Crystallite showing stacking of multiple layers of diamond and graphite. This area shows the 0.206-nm (111 and 1-1-1) fringes of diamond near the top of the image, where layers of graphite and diamond are superposed. This crystallite shows the incomplete nature of the graphite-to-diamond transition.

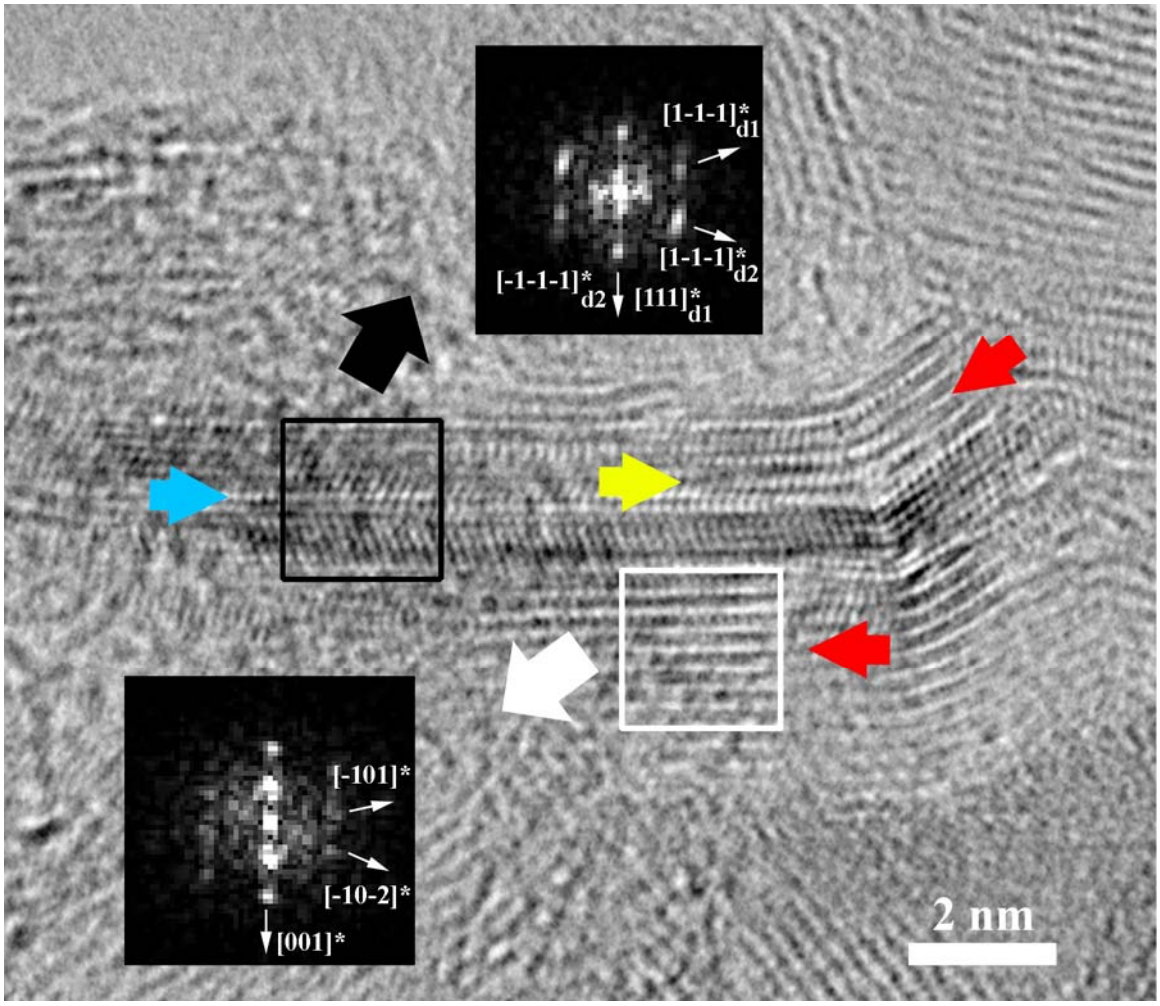

FIGURE 6. HRTEM image of a graphite-diamond particle. The diffractograms for the black- and white-boxed regions are indicated by the black and white arrows, respectively. The diffractogram from the black-boxed region shows twinned diamond (indices according to the two twin individuals: d1 and d2) along $[01\text{-}1]_d$). The blue arrow lies parallel to the twin boundary. The diffractogram from the white-boxed region shows 3R graphite along $[010]_g$. Red arrow – graphite, blue arrow – diamond, and yellow arrow indicates where graphite (00*l*) and diamond (111) fringes meet.

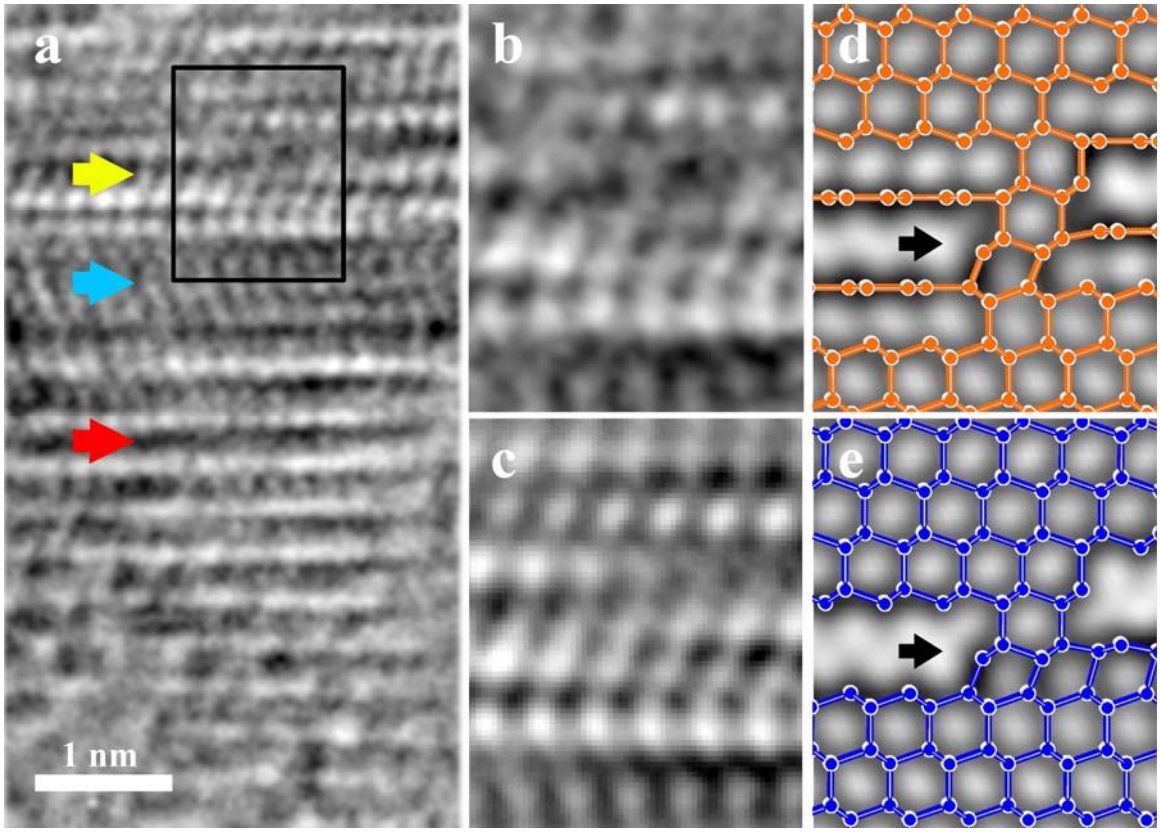

FIGURE 7. Model of the graphite-diamond interface. **(a)** Enlarged area of the HRTEM image of a diamond-graphite particle (yellow arrowed region in Figure 6). Red arrow – graphite, blue arrow – diamond, and yellow arrow indicates where graphite (00*l*) and diamond (111) fringes meet. **(b)** Magnified image of boxed area in **a**. **(c)** Background-filtered area of **b**. **d** and **e,** Structure models and simulated HRTEM images for area **c**. Colored circles mark C atoms. **(d)** Structure model of diamond and interlayered graphite with simulated HRTEM image. **(e)** Structure model of diamond and interlayered graphite-like layers (cf. areas of **d** and **e** indicated by black arrows). The spacing between the C doublets is 0.34 nm, equivalent to the 003 spacings of 3R graphite, but the C doublets have a puckered arrangement of diamond along [0-11].

362

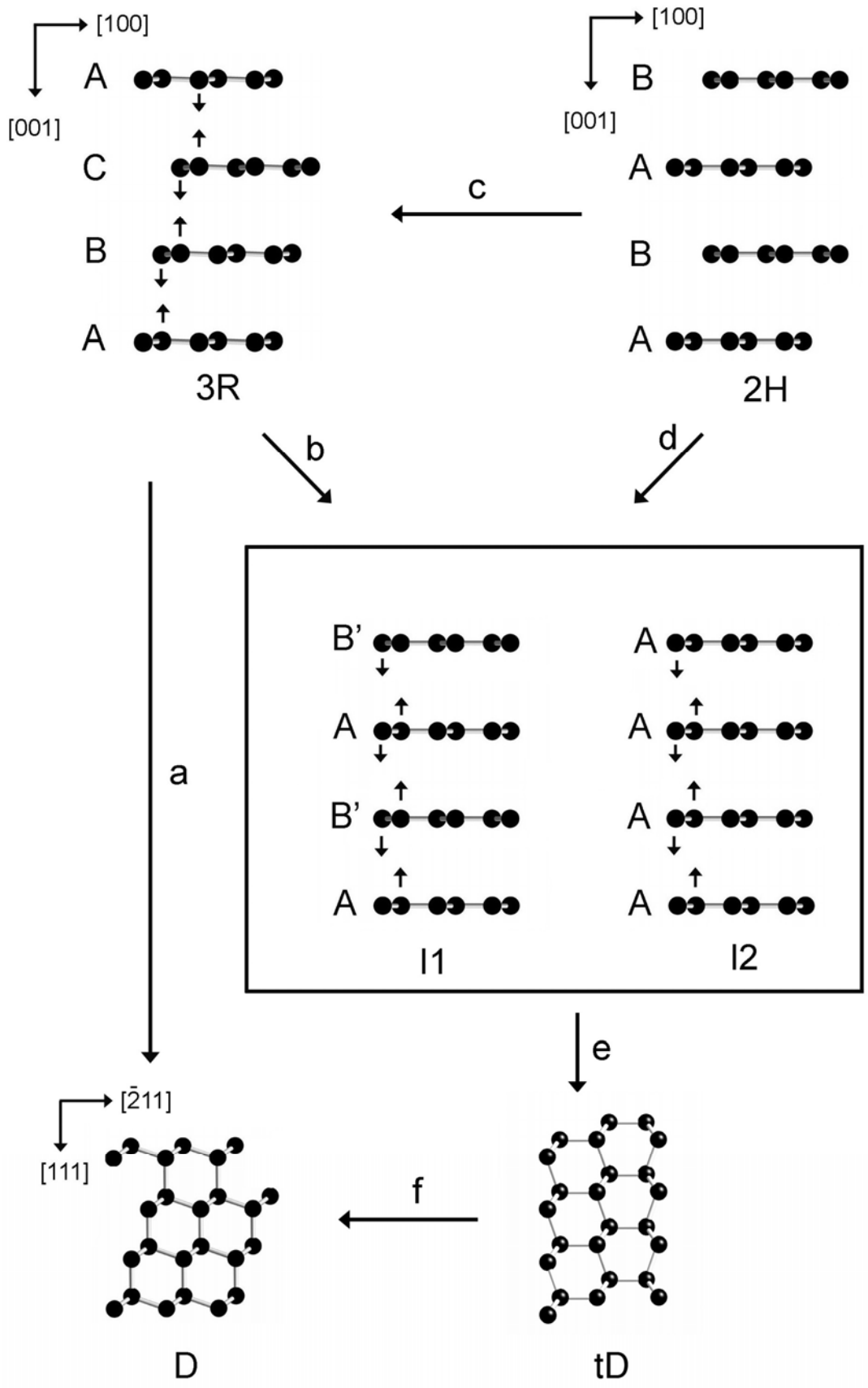

363

364 **FIGURE 8.** Paths for 3R (ABC stacking) and 2H (AB stacking) graphite to
365 diamond (D) and twinned diamond (tD) transformations through buckling and
366 compressions of basal planes**.** 3R transforms to D without (path a) or through
367 intermediate (I1, I2) structures (path b). 2H transforms to diamond through
368 either 3R (path c) or intermediate structures (path d). During further transition,
369 I1 and I2 form tD (path e), which can transform to D (path f).
370
371 ## REFERENCES CITED
372
373

374 Bundy, F.P., Bassett, W.A., Weathers, M.S., Hemley, R.J., Mao, H.K., and
375 Goncharov, A.F. (1996) The pressure-temperature phase and
376 transformation diagram for carbon; Updated through 1994. **Carbon**, 34,
377 141-153.
378 Daulton, T.L., Pinter, N., and Scott, A.C. (2010) No evidence of nanodiamonds in
379 Younger-Dryas sediments to support an impact event. **Proceedings of the**
380 **National Academy of Sciences of the United States of America**, 107,
381 16043-16047.
382 DeCarli, P.S. (1995) Shock wave synthesis of diamond and other phases. In M.D.
383 Drory, D.B. Bogy, M.S. Donley, and J.E. Field, Eds. Mechanical behavior of
384 diamond and other forms of carbon, 383, p. 21-31. Materials Research
385 Society, San Francisco, California.
386 DeCarli, P.S., Bowden, E., Jones, A.P., and Price, G.D. (2002) Laboratory impact
387 experiments versus natural impact events. In C. Koeberl, and K.G.
388 MacLeod, Eds. Catastrophic Events and Mass Extinctions: Impacts and
389 Beyond, 356, p. 595605. Geological Society of America, Boulder.
390 DeCarli, P.S., and Jamieson, J.C. (1961) Formation of diamond by explosive
391 shock. **Science**, 133, 1821-1822.
392 Donnet, J.B., Fousson, E., Wang, T.K., Samirant, M., Baras, C., and Johnson, M.P.
393 (2000) Dynamic synthesis of diamonds. **Diamond and Related Materials**,
394 9, 887-892.
395 Donnet, J.B., Lemoigne, C., Wang, T.K., Peng, C.M., Samirant, M., and Eckhardt,
396 A. (1997) Detonation and shock synthesis of nanodiamonds. **Bulletin de la**
397 **Société Chimique de France**, 134, 875-890.
398 El Goresy, A., Gillet, P., Chen, M., Kunstler, F., Graup, G., and Stahle, V. (2001) In
399 situ discovery of shock-induced graphite-diamond phase transition in
400 gneisses from the Ries Crater, Germany. **American Mineralogist**, 86, 611-
401 621.

Erskine, D.J., and Nellis, W.J. (1991) Shock-induced martensitic phase-transformation of oriented graphite to diamond. **Nature**, 349, 317-319.

Erskine, D.J., and Nellis, W.J. (1992) Shock-induced martensitic-transformation of highy oriented graphite to diamond. **Journal of Applied Physics**, 71, 4882-4886.

Garvie, L.A.J. (2006) Surface electronic states of meteoritic nanodiamonds. **Meteoritics & Planetary Science**, 41, 667-672.

Garvie, L.A.J., and Buseck, P.R. (2004) Nanosized carbon-rich grains in carbonaceous chondrite meteorites. **Earth and Planetary Science Letters**, 224, 431-439.

Garvie, L.A.J., and Buseck, P.R. (2006) Carbonaceous materials in the acid residue from the Orgueil carbonaceous chondrite meteorite. **Meteoritics & Planetary Science**, 41, 633-642.

Harris, P.J.F., and Vis, R.D. (2003) High-resolution transmission electron microscopy of carbon and nanocrystals in the Allende meteorite. **Proceedings of the Royal Society of London Series A**, 459, 2069-2076.

Irifune, T., and Sumiya, H. (2004) Nature of polycrystalline diamond synthesized by direct conversion of graphite using Kawai-type multianvil apparatus. **New Diamond and Frontier Carbon Technology**, 14, 313-327.

Israde-Alcantara, I., Bischoff, J.L., Dominguez-Vazquez, G., Li, H.C., DeCarli, P.S., Bunch, T.E., Wittke, J.H., Weaver, J.C., Firestone, R.B., West, A., Kennett, J.P., Mercer, C., Xie, S.J., Richman, E.K., Kinzie, C.R., and Wolbach, W.S. (2012) Evidence from central Mexico supporting the Younger Dryas extraterrestrial impact hypothesis. **Proceedings of the National Academy of Sciences of the United States of America**, 109, E738-E747.

IUPAC. (1997) Compendium of Chemical Terminology, International Union of Pure and Applied Chemistry. In A.D. McNaught, and A. Wilkinson, Eds. Gold Book. Blackwell Scientific Publications, Oxford.

Kennett, D.J., Kennett, J.P., West, A., Mercer, C., Hee, S.S.Q., Bement, L., Bunch, T.E., Sellers, M., and Wolbach, W.S. (2009a) Nanodiamonds in the Younger Dryas boundary sediment layer. **Science**, 323, 94-94.

Kennett, D.J., Kennett, J.P., West, A., West, G.J., Bunch, T.E., Culleton, B.J., Erlandson, J.M., Hee, S.S.Q., Johnson, J.R., Mercer, C., Shen, F., Sellers, M., Stafford, T.W., Stich, A., Weaver, J.C., Wittke, J.H., and Wolbach, W.S. (2009b) Shock-synthesized hexagonal diamonds in Younger Dryas boundary sediments. **Proceedings of the National Academy of Sciences of the United States of America**, 106, 12623-12628.

Khaliullin, R.Z., Eshet, H., Kuhne, T.D., Behler, J., and Parrinello, M. (2011) Nucleation mechanism for the direct graphite-to-diamond phase transition. **Nature Materials**, 10, 693-697.

Kurbatov, A.V., Mayewski, P.A., Steffensen, J.P., West, A., Kennett, D.J., Kennett, J.P., Bunch, T.E., Handley, M., Introne, D.S., Hee, S.S.Q., Mercer, C.,

Sellers, M., Shen, F., Sneed, S.B., Weaver, J.C., Wittke, J.H., Stafford, T.W., Donovan, J.J., Xie, S.J., Razink, J.J., Stich, A., Kinzie, C.R., and Wolbach, W.S. (2010) Discovery of a nanodiamond-rich layer in the Greenland ice sheet. **Journal of Glaciology**, 56, 747-757.

Langenhorst, F., Shafranovsky, G.I., Masaitis, V.L., and Koivisto, M. (1999) Discovery of impact diamonds in a Fennoscandian crater and evidence for their genesis by solid-state transformation. **Geology**, 27, 747-750.

Le Guillou, C., Brunet, F., Irifune, T., Ohfuji, H., and Rouzaud, J.N. (2007) Nanodiamond nucleation below 2273 K at 15 GPa from carbons with different structural organizations. **Carbon**, 45, 636-648.

Le Guillou, C., Rouzaud, J.N., Remusat, L., Jambon, A., and Bourot-Denise, M. (2010) Structures, origin and evolution of various carbon phases in the ureilite Northwest Africa 4742 compared with laboratory-shocked graphite. **Geochimica Et Cosmochimica Acta**, 74, 4167-4185.

Lipson, H., and Stokes, A.R. (1942) The structure of graphite. **Proceedings of the Royal Society of London Series A - Mathematical and Physical Sciences**, 181, 0101-0105.

Mostefaoui, S., El Goresy, A., Hoppe, P., Gillet, P., and Ott, U. (2002) Mode of occurrence, textural settings and nitrogen-isotopic compositions of in situ diamonds and other carbon phases in the Bencubbin meteorite. **Earth and Planetary Science Letters**, 204, 89-100.

Mykhaylyk, O.O., Solonin, Y.M., Batchelder, D.N., and Brydson, R. (2005) Transformation of nanodiamond into carbon onions: a comparative study by high-resolution transmission electron microscopy, electron energy-loss spectroscopy, x-ray diffraction, small-angle x-ray scattering, and ultraviolet Raman spectroscopy. **Journal of Applied Physics**, 97, Art. No. 074302.

Nakamura-Messenger, K., Messenger, S., Keller, L.P., Clemett, S.J., and Zolensky, M.E. (2006) Organic globules in the Tagish Lake meteorite: remnants of the protosolar disk. **Science**, 314, 1439-1442.

Nakamuta, Y., and Toh, S. (2013) Transformation of graphite to lonsdaleite and diamond in the Goalpara ureilite directly observed by TEM. **American Mineralogist**, 98, 574-581.

Pratesi, G., Lo Giudice, A., Vishnevsky, S., Manfredotti, C., and Cipriani, C. (2003) Cathodoluminescence investigations on the Popigai, Ries, and Lappajdrvi impact diamonds. **American Mineralogist**, 88, 1778-1787.

Rubin, A.E., Kallemeyn, G.W., Wasson, J.T., Clayton, R.N., Mayeda, T.K., Grady, M., Verchovsky, A.B., Eugster, O., and Lorenzetti, S. (2003) Formation of metal and silicate globules in Gujba: A new Bencubbin-like meteorite fall. **Geochimica et Cosmochimica Acta**, 67, 3283-3298.

Scandolo, S., Bernasconi, M., Chiarotti, G.L., Focher, P., and Tosatti, E. (1995) Pressure-induced transformation path of graphite to diamond. **Physical Review Letters**, 74, 4015-4018.

Sharp, T.G., and DeCarli, P.S. (2006) Shock Effects in Meteorites. In D.S.M.J. Lauretta, H.Y., Ed. Meteorites and the Early Solar System II, p. 653-678. The University of Arizona Press.

Sumiya, H., Yusa, H., Inoue, T., Ofuji, H., and Irifune, T. (2006) Conditions and mechanism of formation of nano-polycrystalline diamonds on direct transformation from graphite and non-graphitic carbon at high pressure and temperature. **High Pressure Research**, 26, 63-69.

Weisberg, M.K., and Kimura, M. (2004) Petrology and Raman spectroscopy of shock phases in the Gujba CB chondrite and the shock history of hte CB parent body. **Lunar and Planetary Science Conference**, XXXV, Abstract#1599.

Weisberg, M.K., Kimura, M., Suzuki, A., Ohtani, E., and Sugiura, N. (2006) Discovery of coesite and significance of high pressure phases in the Gujba CB chondrite. **Lunar and Planetary Science Conference**, XXXVII, Abstract#1788.

Wyckoff, R.W.G. (1963) Crystal structures. Interscience Publishers, New York.

Yagi, T., Utsumi, W., Yamakata, M., Kikegawa, T., and Shimomura, O. (1992) High-pressure diffracton study of the phase-transformation from graphite to hexagonal diamond at room temperature. **Physical Review B**, 46, 6031-6039.

Yamada, K., Tanabe, Y., and Sawaoka, A.B. (2000) Allotropes of carbon shock synthesized at pressures up to 15GPa. **Philosophical Magazine A - Physics of Condensed Matter Structure Defects and Mechanical Properties**, 80, 1811-1828.

Yang, G.W., and Wang, J.B. (2001) Pulsed-laser-induced transformation path of graphite to diamond via an intermediate rhombohedral graphite. **Applied Physics a-Materials Science & Processing**, 72, 475-479.

Yelisseyev, A., Meng, G.S., Afanasyev, V., Pokhilenko, N., Pustovarov, V., Isakova, A., Lin, Z.S., and Lin, H.Q. (2013) Optical properties of impact diamonds from the Popigai astrobleme. **Diamond and Related Materials**, 37, 8-16.

Zou, Q., Wang, M.Z., Li, Y.G., Lv, B., and Zhao, Y.C. (2010) HRTEM and Raman characterisation of the onion-like carbon synthesised by annealing detonation nanodiamond at lower temperature and vacuum. **Journal of Experimental Nanoscience**, 5, 473-487.

Appendix 1

Derivation of the graphite to diamond transition matrices

For 2H graphite (g2H), we measured the following node overlaps, 003_g and 111_d, 300_g and $4\text{-}2\text{-}2_d$, and $1\text{-}20_g$ and $0\text{-}22_d$, and developed the matrix equations:

$$\begin{pmatrix} a_{11} & a_{12} & a_{13} \\ a_{21} & a_{22} & a_{23} \\ a_{31} & a_{32} & a_{33} \end{pmatrix}\begin{pmatrix} 0 \\ 0 \\ 3 \end{pmatrix}_{g2H} = \begin{pmatrix} 1 \\ 1 \\ 1 \end{pmatrix}_{d}$$

$$\begin{pmatrix} a_{11} & a_{12} & a_{13} \\ a_{21} & a_{22} & a_{23} \\ a_{31} & a_{32} & a_{33} \end{pmatrix}\begin{pmatrix} 3 \\ 0 \\ 0 \end{pmatrix}_{g2H} = \begin{pmatrix} 4 \\ -2 \\ -2 \end{pmatrix}_{d}$$

$$\begin{pmatrix} a_{11} & a_{12} & a_{13} \\ a_{21} & a_{22} & a_{23} \\ a_{31} & a_{32} & a_{33} \end{pmatrix}\begin{pmatrix} 1 \\ -2 \\ 0 \end{pmatrix}_{g2H} = \begin{pmatrix} 0 \\ -2 \\ 2 \end{pmatrix}_{d}$$

Solving for a_{ij} gives the transition matrix for 2H graphite:

$$\begin{pmatrix} \frac{4}{3} & \frac{2}{3} & \frac{1}{3} \\ \frac{-2}{3} & \frac{2}{3} & \frac{1}{3} \\ \frac{-2}{3} & \frac{-4}{3} & \frac{1}{3} \end{pmatrix} = \frac{1}{3}\begin{pmatrix} 4 & 2 & 1 \\ -2 & 2 & 1 \\ -2 & -4 & 1 \end{pmatrix}$$

For 3R graphite (g3R), we measured the following node overlaps, 009_g and 222_d, 300_g and $4\text{-}2\text{-}2_d$, and $1\text{-}20_g$ and $0\text{-}22_d$, and developed the matrix equations:

$$\begin{pmatrix} a_{11} & a_{12} & a_{13} \\ a_{21} & a_{22} & a_{23} \\ a_{31} & a_{32} & a_{33} \end{pmatrix}\begin{pmatrix} 0 \\ 0 \\ 9 \end{pmatrix}_{g3R} = \begin{pmatrix} 2 \\ 2 \\ 2 \end{pmatrix}_{d}$$

549
$$\begin{pmatrix} a_{11} & a_{12} & a_{13} \\ a_{21} & a_{22} & a_{23} \\ a_{31} & a_{32} & a_{33} \end{pmatrix}\begin{pmatrix} 3 \\ 0 \\ 0 \end{pmatrix}_{g3R} = \begin{pmatrix} 4 \\ -2 \\ -2 \end{pmatrix}_{d}$$

550
$$\begin{pmatrix} a_{11} & a_{12} & a_{13} \\ a_{21} & a_{22} & a_{23} \\ a_{31} & a_{32} & a_{33} \end{pmatrix}\begin{pmatrix} 1 \\ -2 \\ 0 \end{pmatrix}_{g3R} = \begin{pmatrix} 0 \\ -2 \\ 2 \end{pmatrix}_{d}$$

551

552 Solving for a_{ij} gives the transition matrix for 3R graphite:

553

554
$$\begin{pmatrix} \frac{4}{3} & \frac{2}{3} & \frac{2}{9} \\ \frac{-2}{3} & \frac{2}{3} & \frac{2}{9} \\ \frac{-2}{3} & \frac{-4}{3} & \frac{2}{9} \end{pmatrix} = \frac{2}{9}\begin{pmatrix} 6 & 3 & 1 \\ -3 & 3 & 1 \\ -3 & -4 & 1 \end{pmatrix}$$

555

556

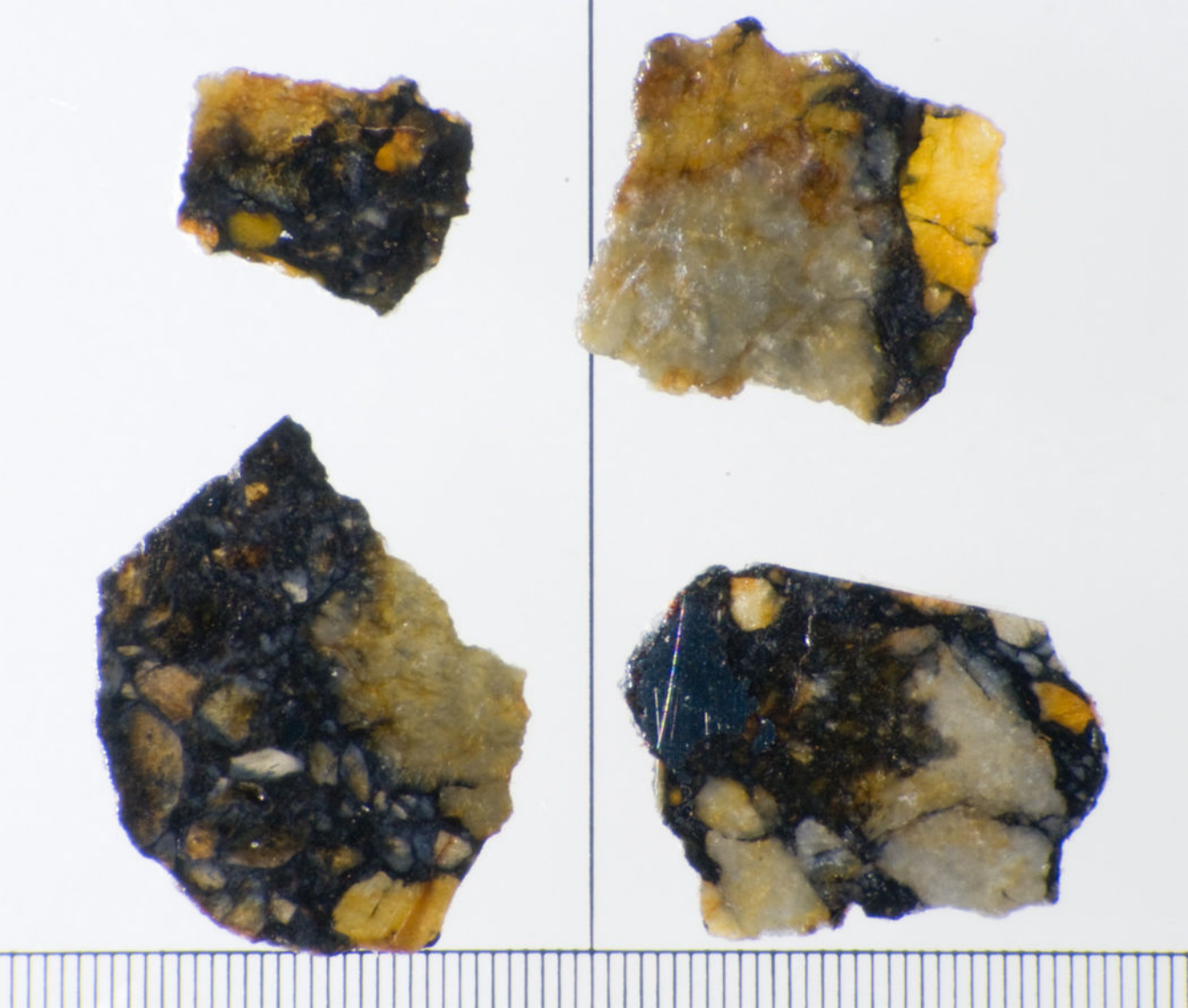

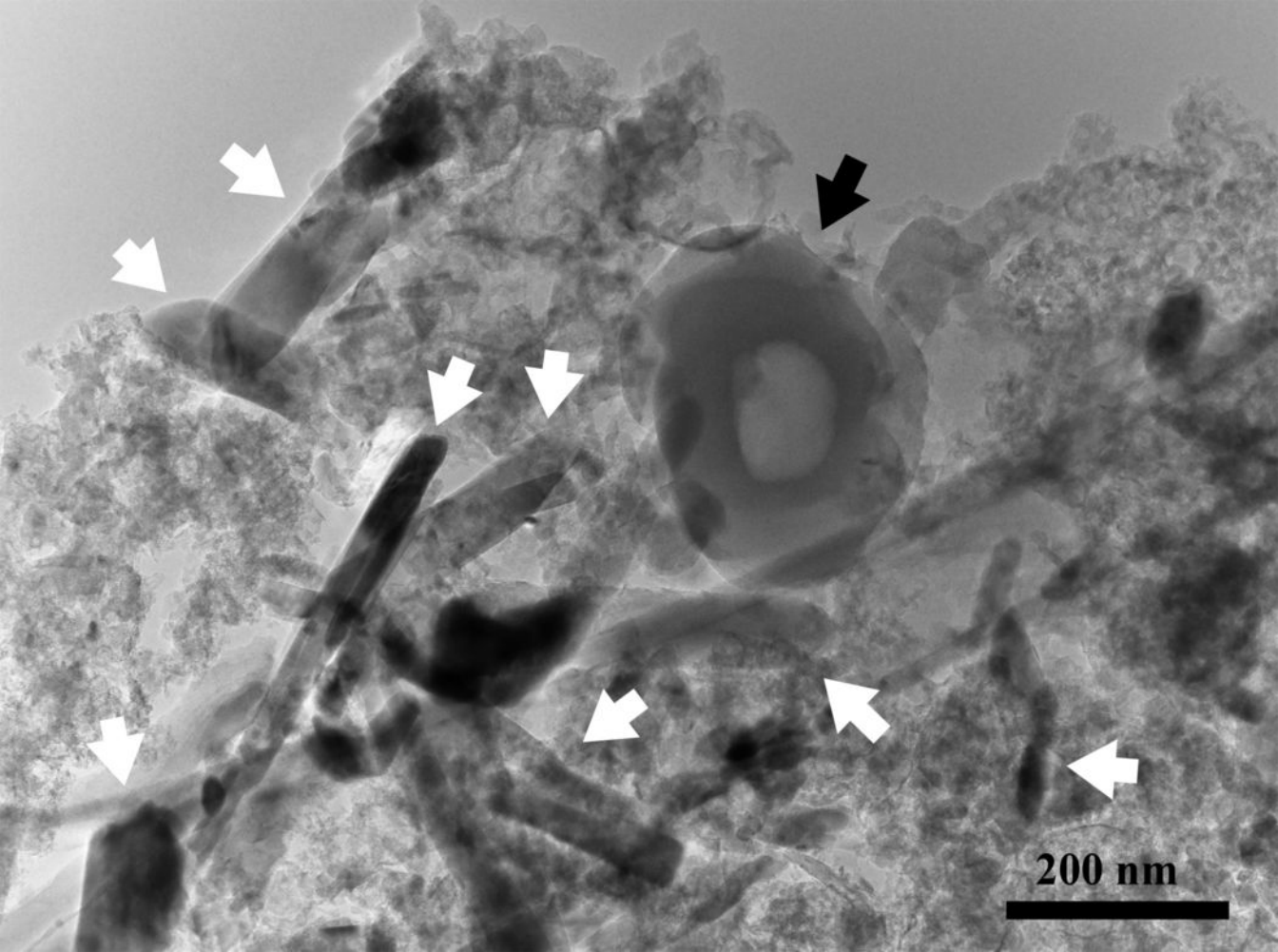
200 nm

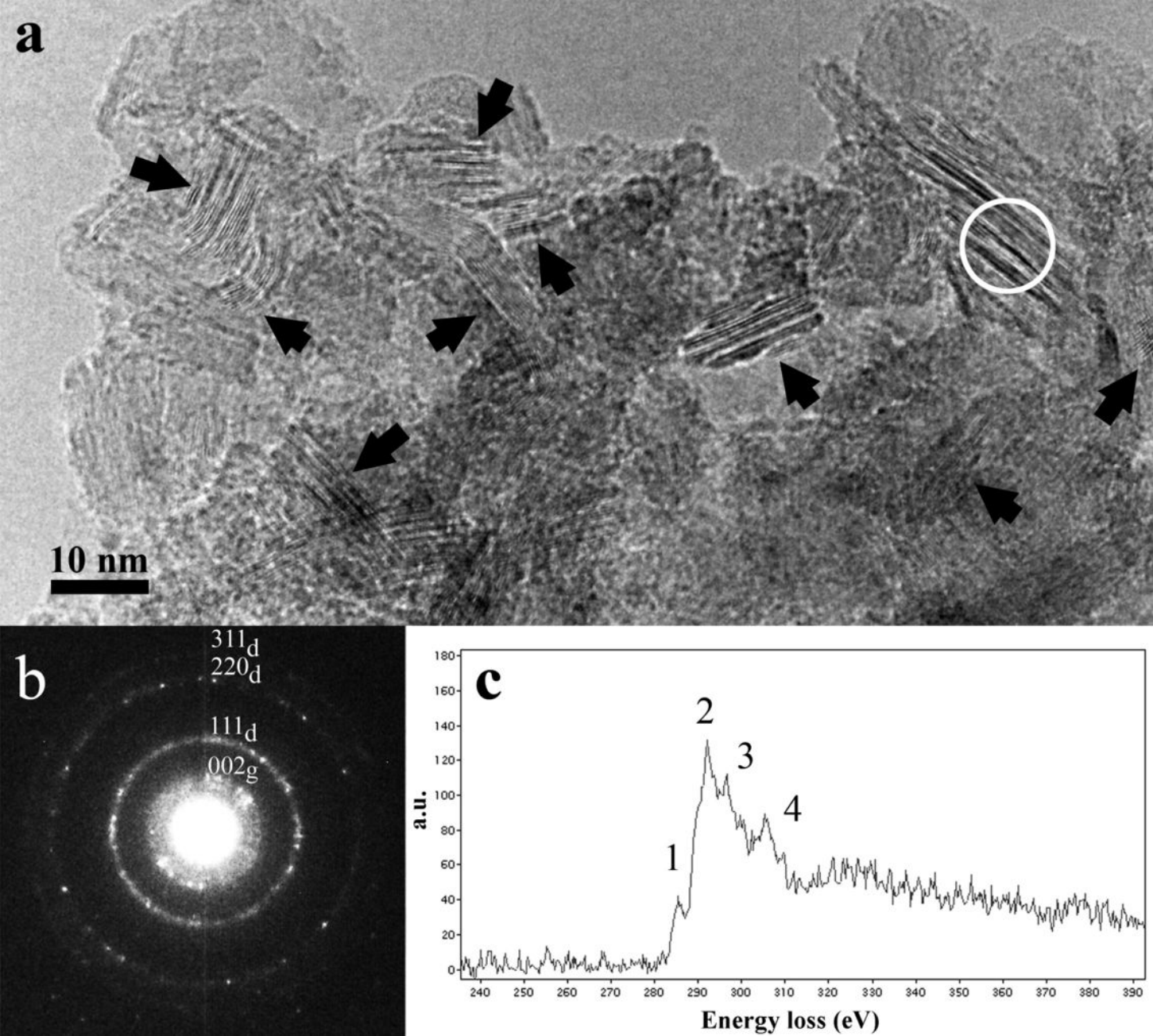
a
10 nm
b
311d
220d
111d
002g
c
a.u.
1
2
3
4
Energy loss (eV)

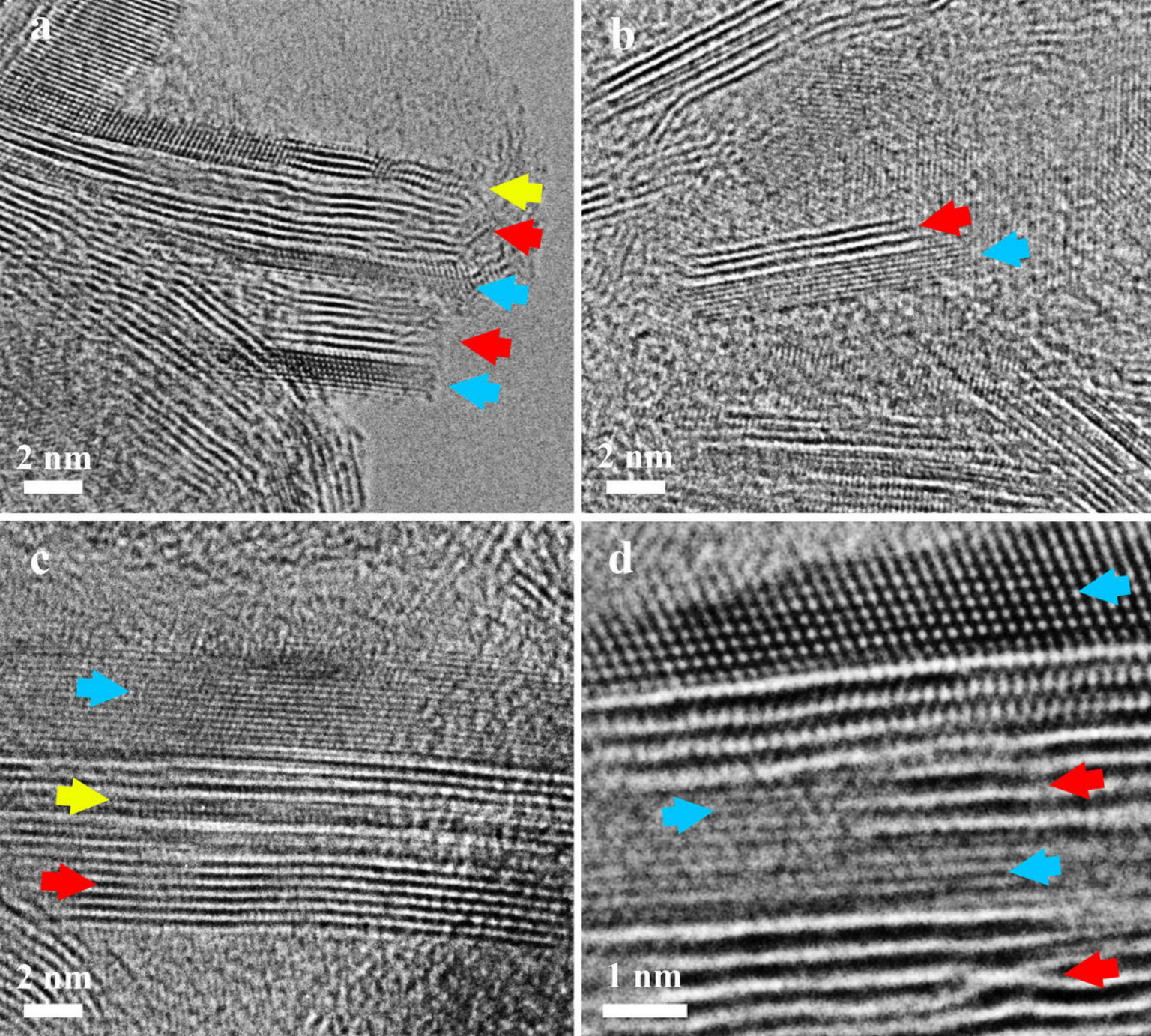
a
2 nm
b
2 nm
c
2 nm
d
1 nm

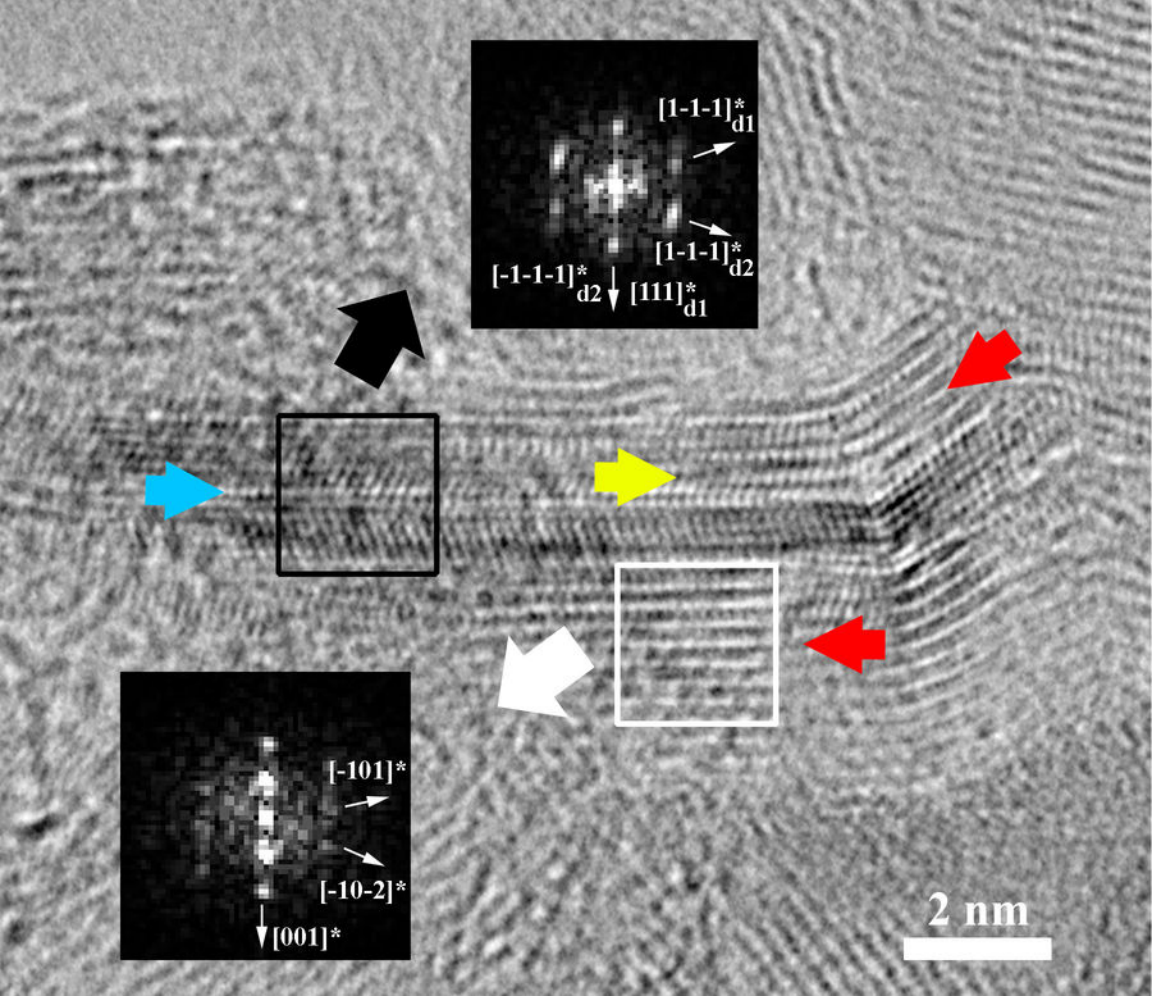
[1-1-1]*d1
[1-1-1]*d2
[-1-1-1]*d2
[111]*d1
[-101]*
[-10-2]*
[001]*
2 nm

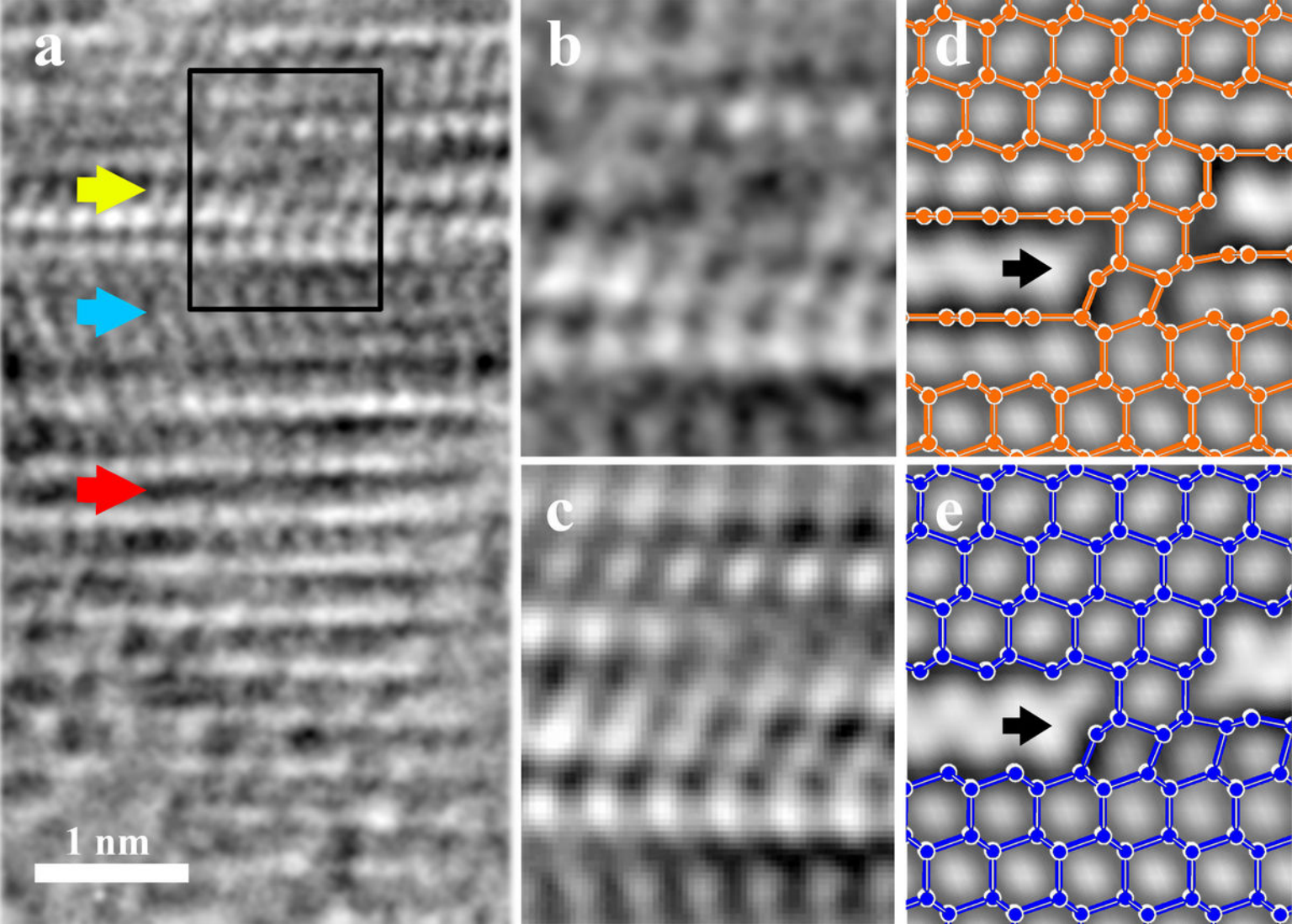
a
b
c
d
e
1 nm

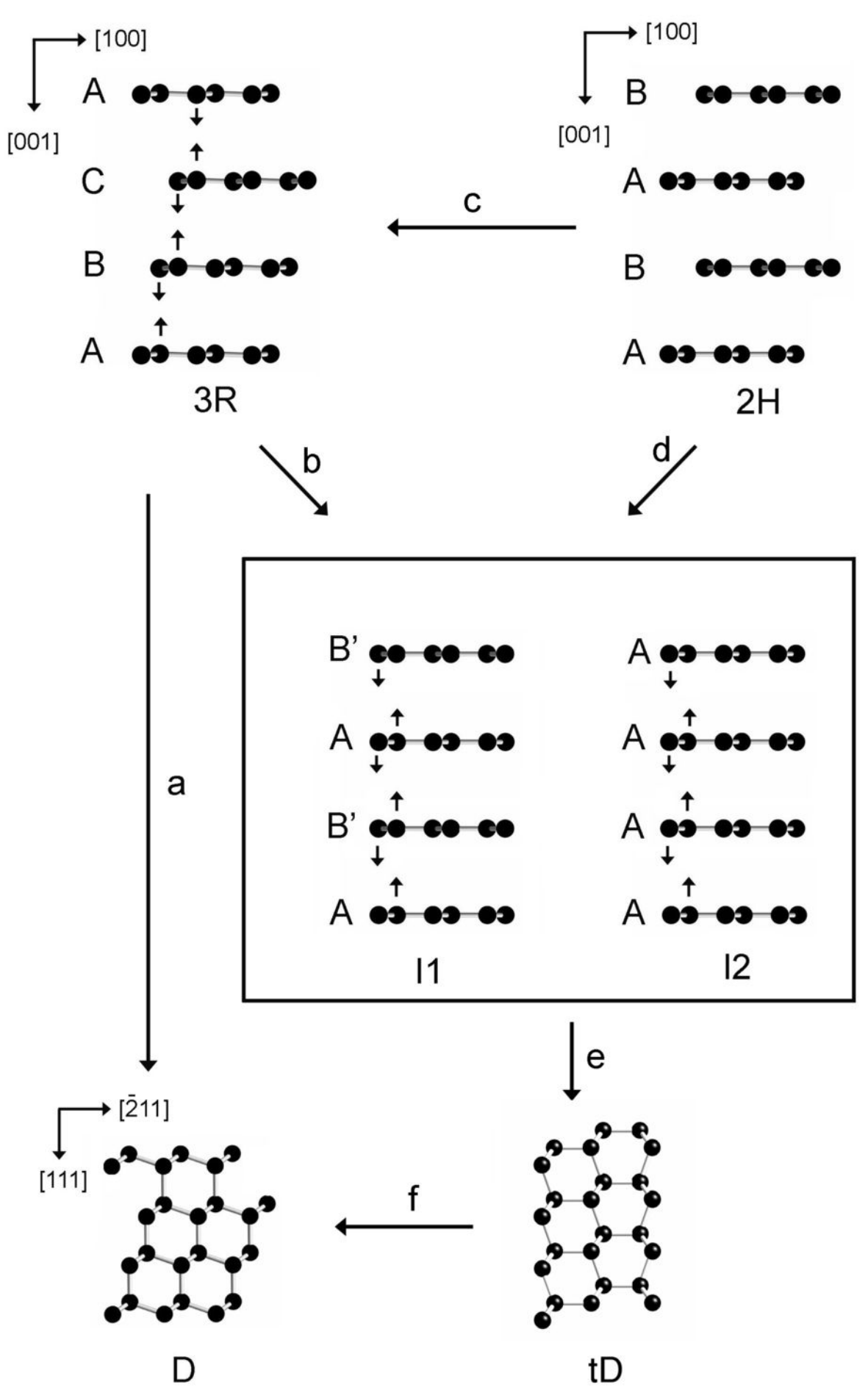
[100]
[001]
A
C
B
A
3R
[100]
[001]
B
A
B
A
2H
c
b
d
a
B'
A
B'
A
I1
A
A
A
A
I2
e
f
[$\bar{2}$11]
[111]
D
tD